U. S. Army NVESD MWIR Polarization Research for Ground Targets

James D. Howe and Rudolph G. Buser
U. S. Army NVESD, Ft. Belvoir, VA

ABSTRACT

Previous infrared polarization imaging research has shown manmade objects to be sources of emitted and reflected polarized radiation while light from natural backgrounds is predominantly unpolarized. The prior work underscored the dramatic improvements in signal to clutter ratio that could be achieved in a typical target acquisition scenario using polarization sensing techniques.

The U. S. Army Night Vision and Electronic Sensors Directorate has developed complete Stokes imaging polarimeters in an effort to investigate polarization phenomenology and to quantify expected improvements to target acquisition and mine detection.

While polarization due to reflection in the visible spectrum has been studied more and is better understood, in this paper we concentrate on polarization due to reflection and emission in the infrared since we are interested in technology with tactical utility and thus twenty-four hour capability. After a brief review of IR polarization phenomenology and a short summary of previous work this paper will review the design and calibration of one of our infrared polarization cameras. Example phenomenology studies of MWIR polarization from surface scattered landmines and from ground targets at tactically relevant ranges will be presented.

1. Introduction

1.1 Polarization Phenomenology

The reflectance properties of smooth surfaces are described by the Fresnel equations. [Bennett]. For specular materials the polarized emittance is one minus the polarized reflectance. The polarized radiance in the thermal IR is composed of polarized thermal emission and polarized reflection. The emission is preferentially polarized parallel to the plane of incidence defined by the surface normal and the camera (perpendicular to the target facet), while the reflection of background (sun, sky, trees, etc.) is preferentially polarized perpendicular to the plane of incidence.

The horizontal and vertical components of radiance due to both emission and reflection from a horizontal target surface are

$$L_{\perp} = \frac{1}{2}\varepsilon_{\perp} L_{BB}(T_{Tgt}) + \frac{1}{2}\rho_{\perp} L(T_{Bkg})$$

$$L_{\parallel} = \frac{1}{2}\varepsilon_{\parallel} L_{BB}(T_{Tgt}) + \frac{1}{2}\rho_{\parallel} L(T_{Bkg})$$

Howe, J.D.; Buser, R.G. (2005) U. S. Army NVESD MWIR Polarization Research for Ground Targets. In *Emerging EO Phenomenology* (pp. 21-1 – 21-18). Meeting Proceedings RTO-MP-SET-094, Paper 21. Neuilly-sur-Seine, France: RTO. Available from: http://www.rto.nato.int/abstracts.asp.

where $L_{BB}(T_{Tgt})$ is the radiance from the target and $L_{BB}(T_{Bkg})$ is the radiance from the background incident on the target. ε and ρ are the emittance and reflectance, and ε = 1 – ρ. Parallel and perpendicular orientations here refer to the target facet.

And the linearly polarized radiance is

$$L_{Pol} = L_{\perp} - L_{\parallel}$$

$$L_{Pol} = \frac{1}{2}(\varepsilon_{\perp} - \varepsilon_{\parallel})[L_{BB}(T_{Tgt}) - L(T_{Bkg})]$$

1.2.1 Previous work

Some of the earliest work in the U.S. on polarization imaging of infrared radiation began the early 1960's and involved serially scanned InSb detectors and rotating linear polarizers. The camera sensitivity was low compared to parallel-scanned or staring focal plane array (FPA)-based sensors. Polarization components of a pixel were measured in temporal sequence, not simultaneously, and exact spatial registration was difficult for a variety of reasons. The resulting polarization image quality was relatively poor. Even so, the early studies showed that emissive polarization had promise in tactical applications, especially as a cue to manmade objects.

Later IR polarization imaging system designs had more sensitivity and were based on discrete serial-parallel-scanned, as well as SPRITE-based [Lewis] system designs. More recent designs exploit the higher sensitivity of staring FPAs. Polarization analyzing elements for such system designs often have been placed in the optical train outside the detector Dewar. Recently, efforts have been directed toward placing the analyzers in the Dewar very near, or directly on a parallel-scanned or staring FPA [Chun] in order to allow nearly simultaneous or exactly simultaneous measurements of all polarization components, to improve spatial registration between measurements, and to improve sensitivity.

Recent studies have resulted in greatly improved understanding of polarimetry capabilities: man-made target cueing, enhanced change detection, and the ability to provide shape information. We have also learned about the tradeoffs between MWIR and LWIR bands for different applications and we have a greater understanding of the sensing requirements (e.g. sensitivity, channel registration, calibration, simultaneity).

Polarization has been found to provide complementary information to that of hyperspectral sensing: for example, where hyperspectral sensing can indicate the pigment properties of the paint on a vehicle, polarization is more of an indicator of surface roughness.

2. PASSIVE POLARIMETRY

Polarimetry is a measurement technique which involves processing multiple intensity measurements of electromagnetic radiation into a 4-element Stokes vector. This Stokes vector, which completely characterizes the polarization state of the radiation, consists of four elements [S0, S1, S2, S3], where S0 is the intensity of the radiation, S1 is the difference between horizontal and vertical intensity components, S2 is the difference between 45-degree and 135-degree intensity components, and S3 is the difference between the right-circularly-polarized and left-circularly-polarized components. More physically intuitive quantities exist to describe polarized light, all of which may be computed from Stokes vector elements, such as the degree of polarization (DoP), degree of linear polarization (DoLP), degree of circular polarization (DoCP), and the orientation of the major axis of the polarization ellipse. These properties are computed using the following equations:

$$DoP = \frac{\sqrt{S_1 + S_2 + S_3}}{S_0}$$

$$DoLP = \frac{\sqrt{S_1 + S_2}}{S_0}$$

$$DoCP = \frac{S_3}{S_0}$$

$$Orientation = \frac{1}{2}\tan^{-1}\left(\frac{S_2}{S_1}\right)$$

Each of these properties contains unique and important information about the target facet which emitted or reflected the radiation. For instance, degree of polarization can yield information about the roughness and material of the target surface, while orientation can indicate direction of the surface facet normal. Example imagery of Degree of Linear Polarization and Orientation taken using a MWIR polarimeter are shown in Figures 1a and b below. Notice the reflection of the sky off the roof of the HMMWV in Figure 1a. Also notice that the windows appear as a strong manmade facet in the orientation image, Figure 1b, even though the degree of polarization of the windows is low.

In the visible DoLPs can run very high: solar reflections can be near 100%. In the infrared bands typical DoLPs are 5% or less. If the whole MWIR spectral band is used to form a polarization image the polarization signature is often highly variable since it can have both an emissive and a solar reflective component which will depend upon time of day and sun-target-camera angle. The LWIR band has less variable polarization signatures since the signatures are due mostly to emission.

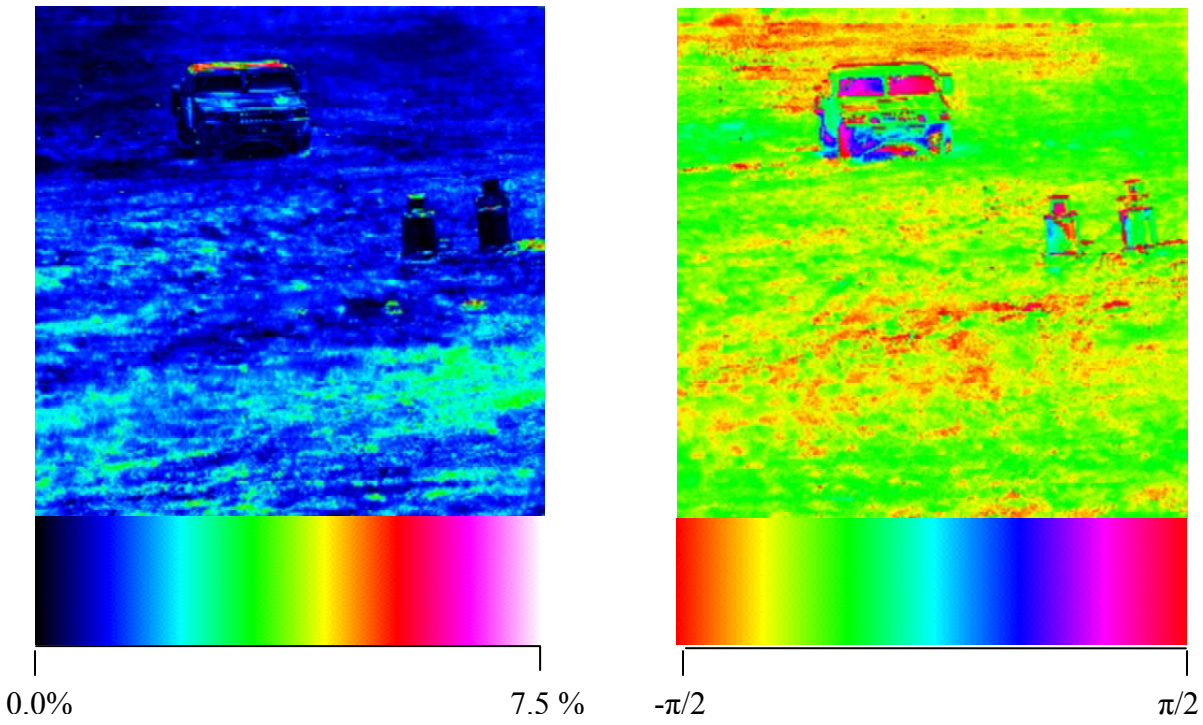

Figure 1a. (left) DoLP of HMMWV and 1b. (right) corresponding orientation image.

3. MWIR SENSOR DESIGN

The MWIR sensor used for the two example studies described in the latter part of this paper is an imaging polarimeter which acquires a complete Stokes vector for every pixel in the scene. Acquiring enough information to determine the complete Stokes vector has advantages when investigating phenomenology but probably is not necessary to produce tactically useful imagery.The polarization analyzer of the sensor is configured in a classical rotating retarder configuration. Fig. 2 shows a block diagram of the instrument which consists of a removable afocal telescope, a rotating quarter-wave linear retarder, a fixed wire grid polarizer, focusing optics, optional spectral filters, and a 512 x 512 pixel 3-5 micron InSb focal plane array (FPA).

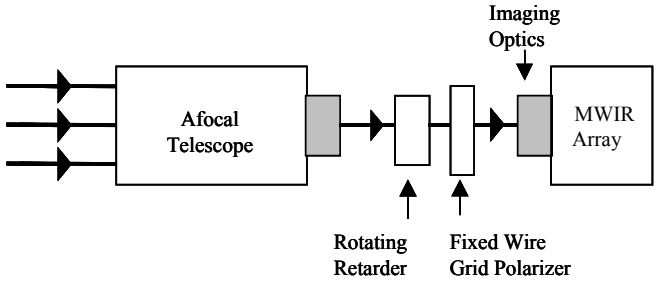

Fig. 2 Block diagram of the MWIR Imaging Polarimeter.

Acquisition of a complete Stokes vector image involves control of several pieces of hardware, a process automated by a custom software package. During a measurement sequence, the retarder is rotated through 360^{o} in order to suppress false polarization at target edges [Smith, 1999, Howe, 1999], and images are acquired at every 22.5^{o}. This results in 16 intensity images, which are then processed into a Stokes vector for every pixel in the scene via the data reduction matrix (DRM) of the system [Smith, 2000]. The set of 16 intensity values for each pixel is referred to as its measurement vector. The DRM is created based on the known Mueller matrix elements of the polarimeter, which are determined both through measurement of individual element properties and through system calibration.

The polarimeter itself consists of a quarter-wave linear retarder followed by a fixed wire-grid linear polarizer. The polarizer was produced by the deposition of a thin-film metallic grid on a ZnSe substrate. The retarder consists of CdS and CdSe retardation plates whose fast axes are aligned to form a single achromatic quarter-wave plate [Sorinsin]. Care was taken to properly orient the retarder in the rotation stage so as to minimize beam wander due to rotation of the retarder during image acquisition, which could lead to false polarization in the processed Stokes image.

It is necessary to perform a thorough and accurate calibration in order to produce meaningful results with a phenomenology sensor [Smith, 2000]. Calibration is particularly important for an instrument whose data will be used to influence future tactical system designs. In general, calibration of a polarimeter involves collecting Stokes images of a known polarization source. However, because of the inherent ambient temperature dependence of a MWIR sensor, a radiometric calibration needs to be coupled to the polarimetric calibration. Therefore, the calibration process will consist first of a separation of the radiation due to the instrument from flux caused by the scene radiation, followed by a polarimetric calibration using known sources of polarization.

4. EXAMPLE POLARIZATION STUDIES

4.1 MWIR Polarization Signatures of Surface Scattered Mines

4.1.1 Test Description

This series of diurnal passive MWIR polarization signature measurements took place during the winter and early spring months. Testing was done with the sensor on a rooftop of a two-story building. Fig. 6 shows the placement of anti-tank (AT) mines, anti-personnel (AP) mines, and clutter objects, spaced to fill the usable field of view of the sensor. Table 1 lists an identification and characterization of each target. The target array was located 12 meters from the foot of a 15 meter tall building which resulted in a sensor down-look angle of approximately 50 degrees. The sensor was approximately facing eastward. Most of the mines were filled with a material which simulated the proper thermal mass of an explosive-filled mine. The sensor/mine combination was oriented such that trees and sky were the background that reflected off the mines and into the sensor. This observation is important especially in the MWIR because of the delicate

balance between emitted and reflected target radiation whose difference make up a polarization signature.

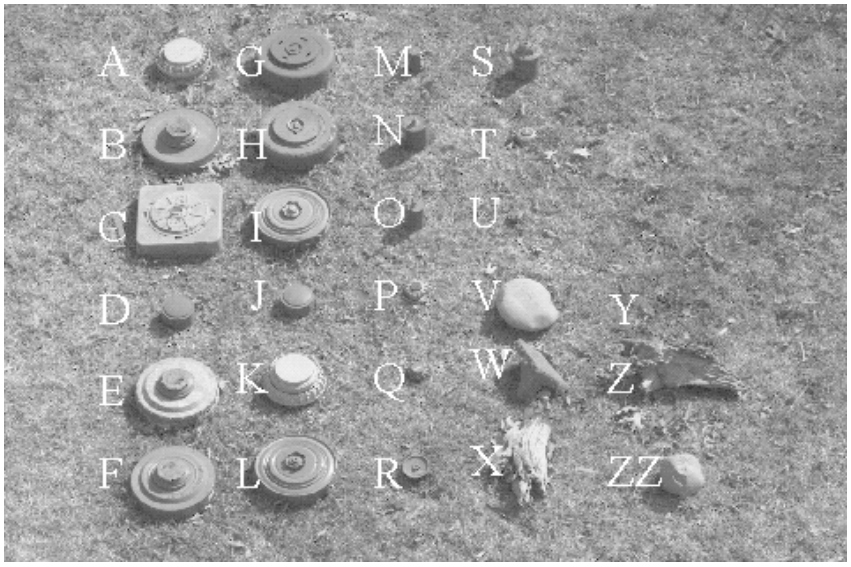

Figure 3. Antitank (AT) mines, Antipersonnel (AP) mines and clutter objects used in this test.

Label	Name	Color	Material	Size
A	VS-1.6	Tan	Plastic	8.5” D, 3” H
B	TM62-P3	Bright green	Metal	12” D, 2.75” H
C	M19	Brown	Plastic	13x13”,3” H
D	RAAM	Green	Metal	5” D, 2.25” H
E	TM62-P2	Pink	Plastic	12” D, 3” H
F	TM62M	Green	Metal	12” D2.5” H
G	M20	Dark green	Metal	12.25” D, 3.5” H
H	M20	Green	Metal	12.25” D, 3.5” H
I	TM46	Green	Metal	12.25” D, 2.75” H
J	RAAM	Green	Metal	12” D, 2.25” H
K	VS-1.6 unfilled	Tan	Plastic	9” D, 4.5” H
L	TM46 unfilled	Green	Metal	12” D, 2.75” H
M	POMZ	Green	Metal	2.5” D, 4” H
N	M16	Green	Metal	4” D, 4.5” H
O	POMZ	Green	Metal	3” D, 4.5” H
P	VS50	Tan	Plastic	3.25” D, 1.5” H
Q	TS50	Green	Plastic	3” D, 1.5” H
R	PMA-3	Green	Plastic	4” D, 1.5” H
S	VAL69	Green	Plastic	4.25” D, 5” H
T	VS50	Tan	Plastic	3.25” D, 1.5” H
U	M19	Green	Plastic	2” D, 1.5” H
V	Stone	Tan	Stone	10” D, 3” H
W	Cement	Grey	Cement	8” L, 4” W, 5” H
X	Wood	Brown	Wood	15”L, 7” W, 3”H
Y	Buried VS-1.6	Tan	Plastic	8.5” D, 3” H
Z	Wood	Brown	Wood	17”L, 4.5” W, 7”H
ZZ	Stone	Tan	Stone	5.5” D, 4” H

Table 1. Mine and confusing object descriptions

Figures 4a, b, c, d show examples of measurements of the minefield taken by the MWIR polarimeter during a period when the ambient temperature dipped below freezing. Figs. 4a and c show intensity (S0) images for day and night, and Figs. 4b and d show the corresponding DoLP images. In the polarization imagery, many of the AT mines are apparent. Those that are not apparent are plastic or smaller mines with rounded tops (e.g. RAAM mines, labeled D and J in Fig. 3). The AP mines are almost impossible to discern. Note that the clutter objects are suppressed as well.

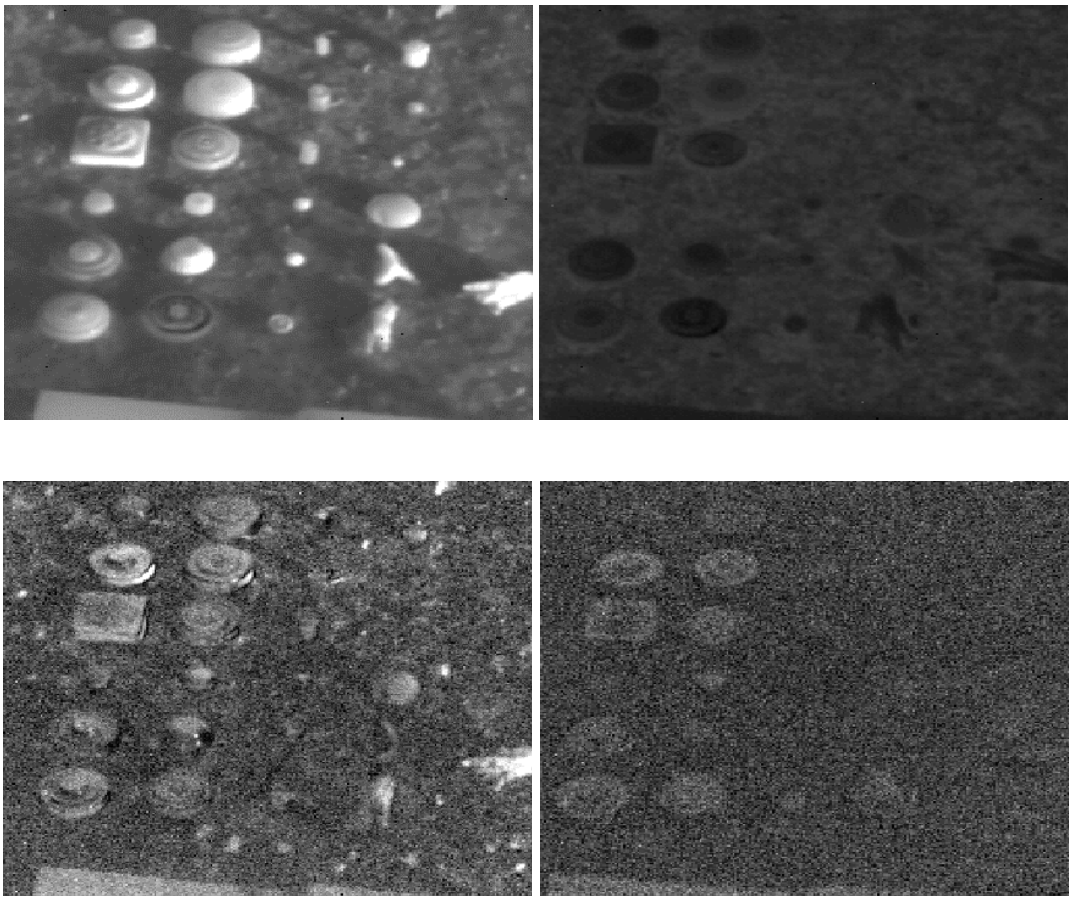

Figures 4a, b, c, d. Intensity (left) and DoLP (right) imagery in daytime (top) and night (bottom)

4.1.2 MWIR Diurnal Measurements

The data indicated that the plastic mines appear somewhat dimmer than the metal mines, both in intensity and in polarization. The thermal contrast normally became negative at night for both types of mines while the polarization contrast remains small but positive through the entire diurnal cycle. The clutter fairly closely tracks the background in DoLP, while it stands out in thermal imagery. As seen in the polarization imagery, the clutter objects tend to disappear while most of the larger mines are still apparent in linear polarization.

Polarization ellipse orientation images of the minefield were also taken, however, they were not particularly informative due to the low DoLPs involved. In all MWIR measurements made, the circular polarization signals are not strong enough to be of utility.

Signal to clutter ratios (SCRs) were calculated both for intensity (S0) signals and DoLP signals. The signal used was the contrast between S0 or DoLP averaged over all mines, and a background level averaged over a representative area. The clutter measure was the variance of a background region including rocks, wood and cinder blocks.

$$SCR = 10 \bullet Log \frac{\left(\overline{Signal} - \overline{Background}\right)^2}{\sigma^2_{Background\&Clutter}}$$

See Figures 5 and 6 which show irradiance and DoLP SCRs. As some of the clutter objects were prominent in the thermal intensity image, the thermal variance within a region including the clutter objects was large. On the other hand, in the DoLP images the clutter objects are very difficult to locate. The background variance in the DoLP images is much less than in the intensity images, indicating background clutter suppression.

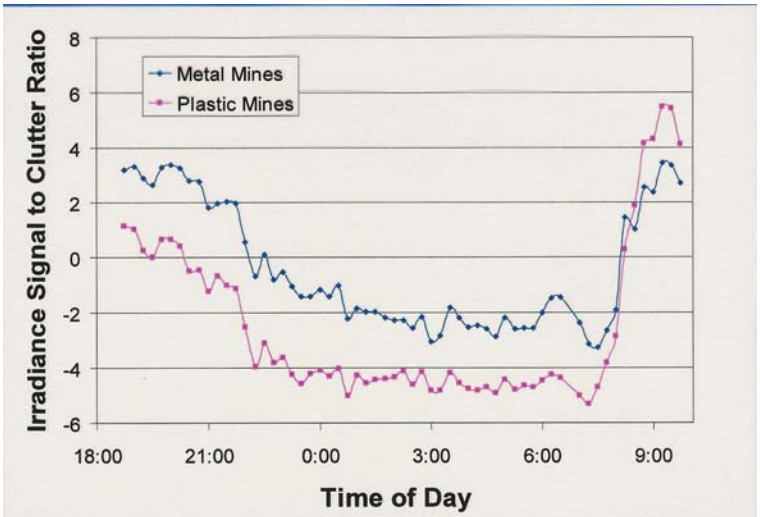

Figure 5. Signal to Clutter Ratio for S0, MWIR irradiance, versus time of day for metal and plastic mines

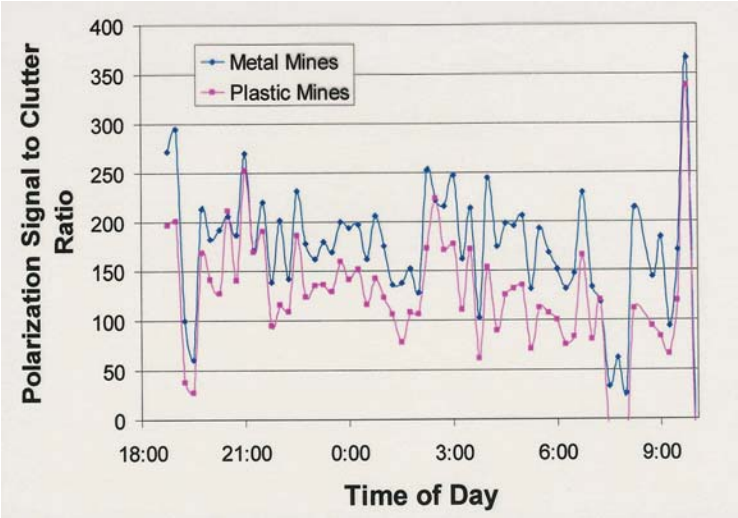

Figure 6. DoLP Signal to Clutter Ratio for metal and plastic mines

The clutter objects also exhibit high contrast in the thermal images, indicating the presence of many confusion objects that would produce false cues in automated detection algorithms. However, the thermal images are sharp and have high target contrast. Thus, after regions of interest are identified, perhaps by a combination of thermal and polarization imagery, the thermal information should be used if further discrimination is necessary. These results indicate that adding the passive polarization information to the thermal would improve detectability of some mines (mainly the large metal mines), and would thus provide a somewhat more robust tactical sensor system.

4.2 Example Study 2: Long Range Target Acquisition

The sensor was operated from within a building on top of a 210 meter hill. Targets were positioned on a plain south of the sensor position (See the “Near” and “Far” sites on the map in figures 8 and 9 below.). Two groups of targets were formed, one at approximately 2.5 kilometers from the sensor and another at approximately 4.7 km. Each target group contained 3 M113s, 3 Howitzers, 2 HMMWVs, and 2 M35A2s. A number of metal panels with different treatments were put at the 2.5 Km site. It is important to note that the solar azimuth sweeps through the target-sensor direction between noon and 13:00 hours each day.

Figures 7 and 8. Target groupings at 2.3 and 4.7 Km showing FOVs revisited.

The sensor was mounted on a high-precision sensor positioning system that allowed rapid, repeatable positioning of the sensor line of sight to within 0.005 degrees. A host computer was used to control the positioning system and camera so that imagery could be acquired from the same fields of view repeatably. The same eight fields of view, five for the 2.5 km site (see figure 7) and 3 for the 4.7 km site (see figure 8), were revisited many times throughout the collection so that the temporal history of the signatures could be documented.

Figure 9. Visible image of one FOV from the 2.5 Km grouping.

The MWIR polarization imagery collection schedule was designed so that signatures were taken throughout one week in November at times from before sunrise through well past thermal crossover, well past sundown. Weather conditions for the week would be categorized as very clear, with only brief times with a thin cloud covering. Visibility was mostly between 60 and 80 km during the day.

4.2.2 Results

Figure 9 shows a visible image of one of the five fields of view within the near target grouping that was repeatedly imaged during the weeklong collection. For the same field of view, examples of false colored imagery of the four stokes components are shown in figures 10 a,b,c,d. The S_0, or intensity, image is simply a typical FLIR image. Notice that background objects and shadows are readily apparent. In the S_1 and S_2 images, backgrounds are suppressed and target facets are highlighted.

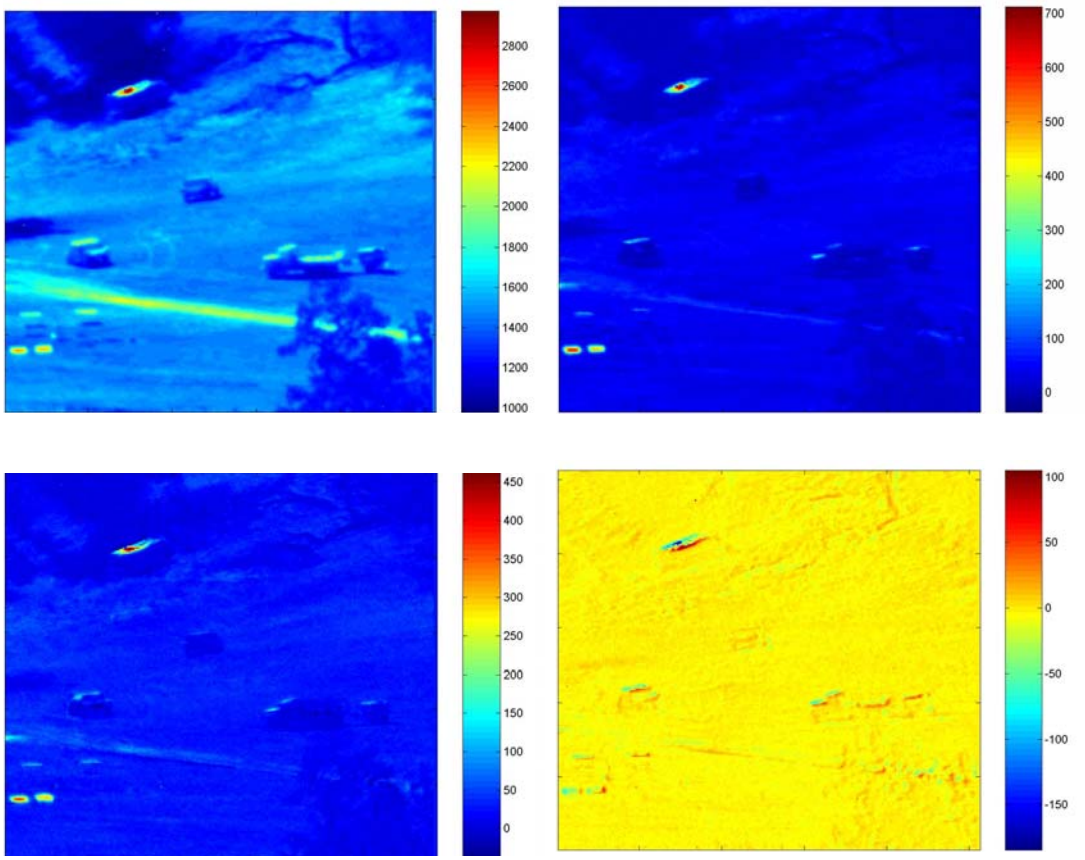

Figure 10 a, b, c, d (top left, top right, bottom left, bottom right) S0, S1, S2, & S3 iamges of a 2.5Km target grouping.

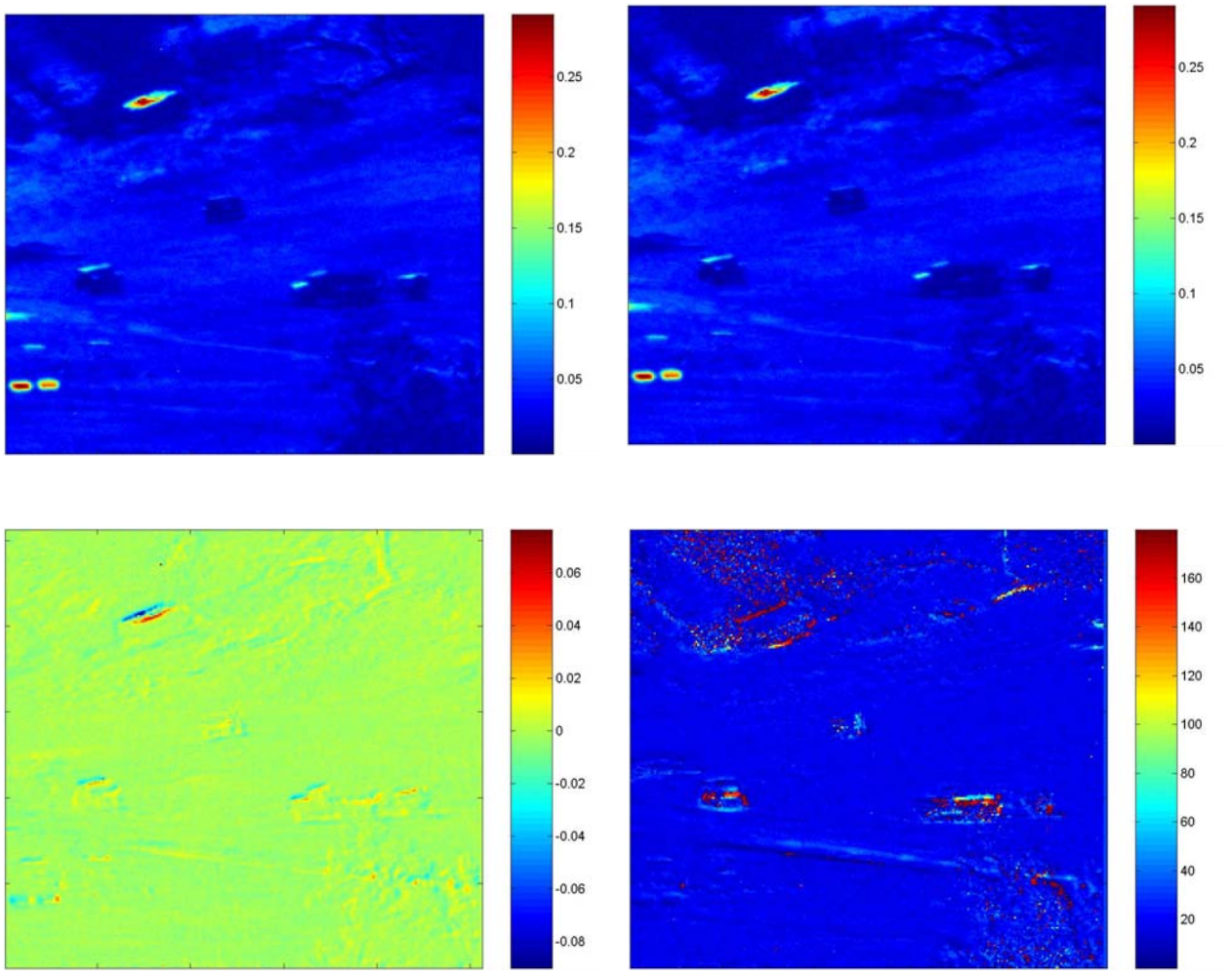

Figure 11 a, b, c, d. - (top left, top rt, bottom left, and bottom rt) DoP, DoLP, DoCP and orientation images of the 2.5km target grouping.

Figures 11 a,b,c,d show false colored imagery of the four derived products, DoP, DoLP, DoCP and orientation. The DoP and DoLP images indicate some very large magnitudes of reflected polarization, ~10% for some of the vehicle hoods and near 25% from the top of the M113A3 and some of the panels.

Figures 12 and 13 show the S_0 (MWIR thermal) image and the DoLP image of the same field of view for six different times during one morning. The images show the strong influence that the sun has on both types of imagery. The S_0 image sequence shows the targets in the sun heating up beginning with the side of the target facing the sun. In the morning sides of targets facing the sun heat first, then horizontal facets as the sun rises in the sky.

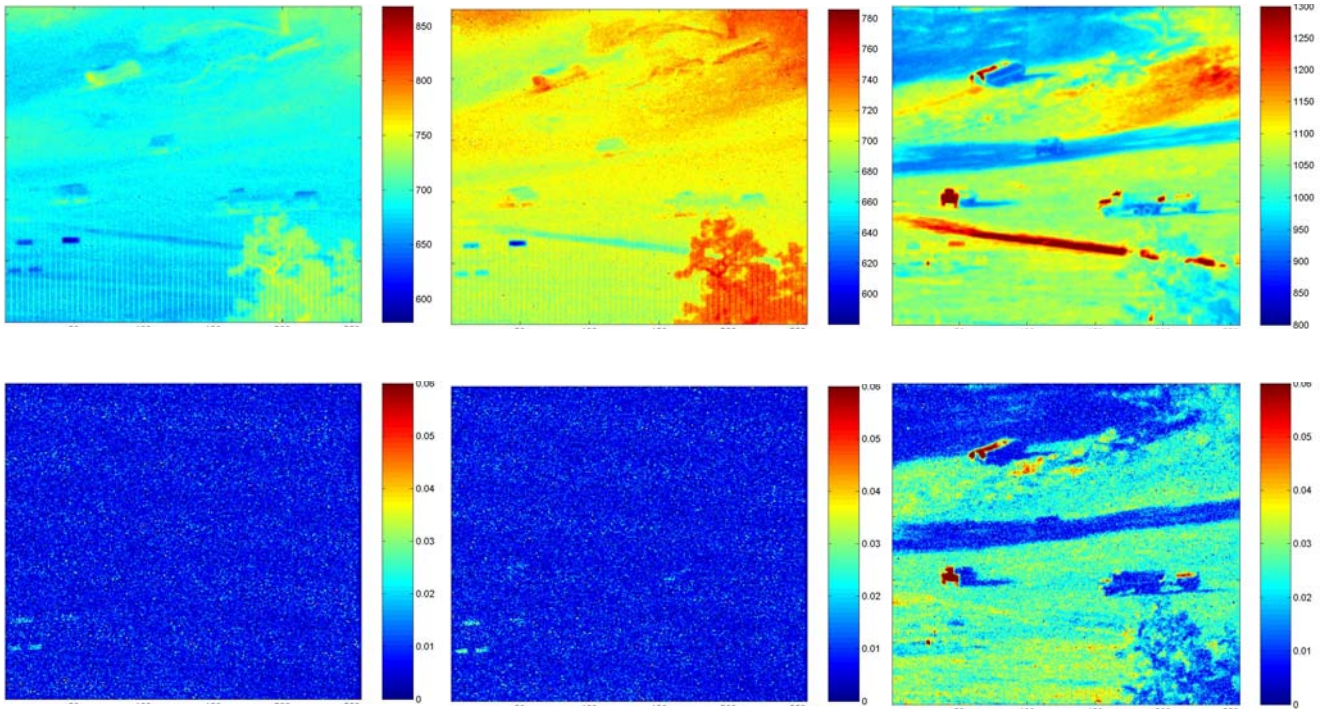

Figure 12 a, b, c, d, e, f. S_0 (top row, a, b, c) and DoLP (bottom row d, e, f) of 2.5 km target grouping at 6:20 (left), 7:06 (center) and 8:20 (right). Units of S_0 are ADUs, and units of DoLP are false colored from 0 - 6%.

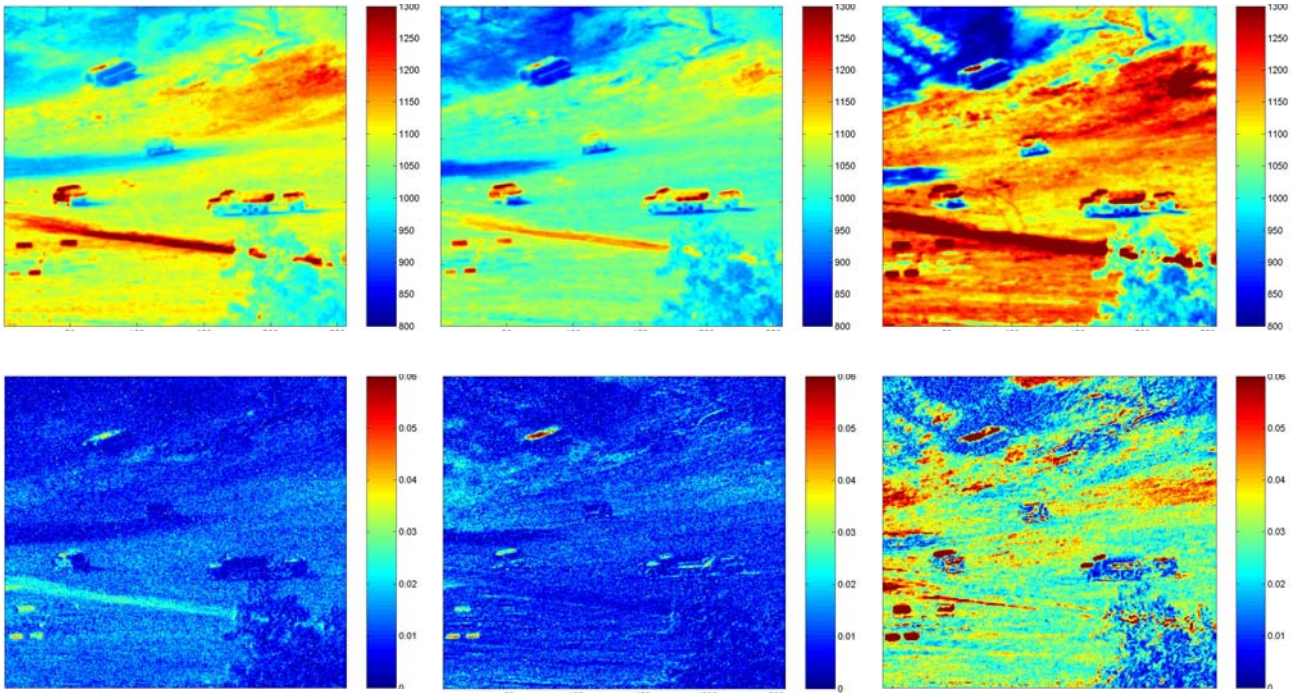

Figure 13 a, b, c, d, e, f S_0 (top row) and DoLP (bottom row) of 2.5 km target grouping at 9:43 (left), 10:43 (center) and 11:16 (right). Units of S_0 are ADUs, and units of DoLP are from 0 - 6%.

Polarization signatures of the sides of some vehicles become large near 8:00 in the morning when the sun - target facet – sensor angle approaches a specular reflection angle. See figure 12, right column. Polarization of the background which is illuminated by the sun is ~2.5%. Vehicles and backgrounds in shadow remain unpolarized. As the sun – target – sensor angle nears the specular reflection angle, the increase in polarization from both the target and background is dramatic.

In order to examine the diurnal properties of the polarization signature we plotted the average DoLP values versus time of day from parts of the image corresponding to different patches of target and background. See figure 14 for an overlay of the patches whose temporal variation of DoLP values are plotted in figure 15.

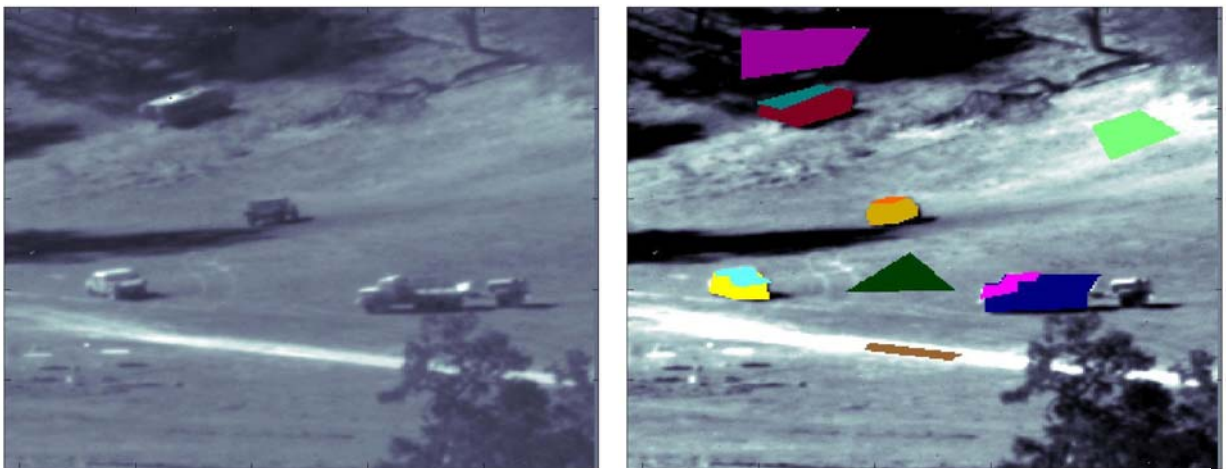

Figure 14. Thermal (S_0) image of 2.5 km target grouping (left) and same image with selected ROIs color coded (right).

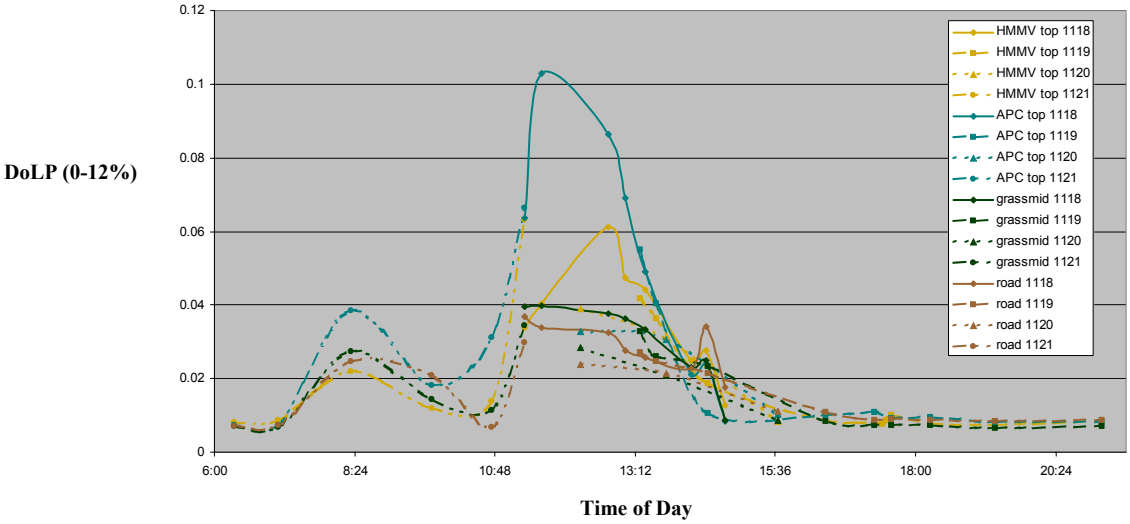

Figure 15. DoLP versus time of day for four different ROIs on four different days.

For times where data from different days is available, magnitudes of the polarization signatures are similar as are their temporal variations. There are some times of day where targets exhibit less polarization than the background. This happens generally when the target is in the shadow.

5.0 CONCLUSIONS

For both the landmine and long range target acquisition examples the polarization signal in the MWIR spectral band is dominated by solar reflections. Magnitudes of the DoLP and the linearly polarized radiance are a strong function of the solar azimuth, peaking sharply when reflections are nearly specular. The dominance of reflection over emissive polarization signatures is also indicated by the direction of the polarization from facets with known orientation. The E field direction was always perpendicular to the facet. We saw no instances of emission dominating the MWIR polarized signature.

The strong variation in the target signature and the very weak night time signature decrease the tactical utility of the MWIR polarization signature, making both man-in-the-loop and automated target discrimination more difficult. The strong dependence of polarized response upon sun – target – camera direction places major restrictions on CONOPS. NVESD has developed a LWIR imaging polarimeter and has begun to explore the tactical utility of LWIR polarization imagery. Since the target and background signatures in the LWIR spectral band are due mostly to emission they will be less variable, easier to predict and hopefully of greater tactical utility.

6.0 REFERENCES

Bennett, Jean M., "Polarization" in Handbook of Optics, Ed., M. Bass ed., (McGraw-Hill, New York, 1993), Chapter 5.

Lewis, G. D. and Jordan, D. L., "Geometrical dart infrared signatures of diffuse and specular darts", in Targets & Backgrounds: Characterization and Representation II, Proc. SPIE 2742, 298-308 (1996).

Chun, C. S. L., Fleming,D. L., Harvey, W. A. and Torok, E. J. "Polarization-Sensitive Infrared Sensor for Target Discrimination", Proc. SPIE 3121, 55-59 (1997).

Smith, M. H., Woodruff, J. B., Howe, J. D., "Beam wander considerations in imaging polarimetry," Proceedings of SPIE Vol. 3754, pp. 50-54, 1999.

Howe, J. D., "Two-color infrared full-Stokes imaging polarimeter development," Proceedings of the IEEE Aerospace Conference, March 6-13, 1999.

Smith, M. H., Howe, J. D., Miller, M. A., Ax, G. R., Blumer, R., "Infrared Stokes polarimeter calibration," Proceedings of SPIE 4133, 2000.

Sornsin, E. A., Chipman, R. A. "Alignment and calibration of an infrared achromatic retarder using FTIR Mueller matrix spectropolarimetry," Proceedings of SPIE Vol. 3121, pp. 28-34, 1997.